

## Manufactured Yttrium Barium Copper Nano Oxide for Medicinal Applications

Article Info:

Article history: Received 2023-05-05 / Accepted 2023-09-28 / Available online 2023-09-28

doi: 10.18540/jcecvl9iss8pp16379-01e



**Rania Daha**

ORCID: <https://Orcid.org/0009-0007-8200-1187>

École Nationale Supérieure des Mines et de la Métallurgie (ENSMM)-Amar Laskri, L3M,  
Chaiba, B.P: 233-RP, 23000 Annaba, Algeria

E-mail: [rania.daha@ensmm-annaba.dz](mailto:rania.daha@ensmm-annaba.dz)

**Manel Bouloudenine**

ORCID: <https://orcid.org/0000-0002-7823-4208>

Mohamed-Cherif Messaadia University, 41000, Souk Ahras, Algeria, LPR, Laboratory, University  
Badji Mokhtar, BP 12, 23000, Annaba, Algeria

E-mail: [m.bouloudenine@univ-soukahras.dz](mailto:m.bouloudenine@univ-soukahras.dz)

**Katia Djenadi**

ORCID: <https://Orcid.org/0000-0002-0513-0985>

Laboratoire de Biochimie Appliquée, Département des Sciences Alimentaires, Faculté des  
Sciences de la Nature et de la Vie, Université de Bejaia, 06000, Bejaia, Algeria,

E-mail: [djenadikatia@yahoo.fr](mailto:djenadikatia@yahoo.fr)

**Tarek Tahraoui**

ORCID: <https://Orcid.org/0000-0002-7815-673X>

École Nationale Supérieure des Mines et de la Métallurgie (ENSMM)-Amar Laskri, L3M,  
Chaiba, B.P: 233-RP, 23000 Annaba, Algeria

E-mail: [tarek.tahraoui@ensmm-annaba.dz](mailto:tarek.tahraoui@ensmm-annaba.dz)

**Stefano Bellucci**

ORCID: <https://Orcid.org/0000-0003-0326-6368>

INFN-Frascati National Laboratories, Rome, Italy

E-mail: [stefano.bellucci@lnf.infn.it](mailto:stefano.bellucci@lnf.infn.it)

**Abdelaziz Rabehi**

ORCID: <https://orcid.org/00000001-8684-4754>

Telecommunications and smart systems Laboratory, University of Ziane Achour, Djelfa 17000,  
Algeria

E-mail: [abdelaziz.rabehi@univ-djelfa.dz](mailto:abdelaziz.rabehi@univ-djelfa.dz)

### Abstract

In light of the considerable interest surrounding the antibacterial properties of nanometal oxides and high-temperature superconductors, this study focuses on the synthesis of  $\text{YBa}_2\text{Cu}_3\text{O}_7$  (YBCO) using the Sol-Gel method. The research delves into the experimental aspects of nanoparticle (NP) synthesis and aims to elucidate the antibacterial potential of YBCO NPs, a high-temperature superconductor, against four distinct bacteria. These bacteria were subjected to varying concentrations of YBCO NPs (0.01 mg/ml, 0.025 mg/ml, 0.05 mg/ml, and 0.1 mg/ml). Comprehensive characterization of the synthesized nanoparticles encompassed techniques such as X-ray diffraction (XRD), scanning electron microscopy (SEM), differential scanning calorimetry (DSC), and thermogravimetric (TG) analysis. Remarkably, the Gram-positive strains, including *Staphylococcus epidermidis* and Methicillin-resistant *Staphylococcus aureus* (MRSA), exhibited pronounced susceptibility to the YBCO NPs, while Gram-negative strains displayed minimal response. Intriguingly, even at elevated concentrations of 0.01, 0.025, 0.05, and 0.1 mg/ml, these

bacterial strains showcased resilient resistance. This research sheds light on the potential of YBCO NPs as an antibacterial agent against specific pathogens.

**Keywords:** YBCO. Nanoparticles. Sol-gel Synthesis. X-Ray diffraction. Antibacterial Activity.

## 1. Introduction

Yttrium Barium Copper Oxide ( $\text{YBa}_2\text{Cu}_3\text{O}_7$ ), often referred to as YBCO, emerges as a notable high-temperature superconductor (HTS), thanks to its exceptional critical temperature surpassing the boiling point of liquid nitrogen (77 K) and its straightforward synthesis under ambient conditions (Sun *et al.*, 1987). The intricate composition of  $\text{YBa}_2\text{Cu}_3\text{O}_{7-\delta}$  intricately intertwines with the YBCO-123 superconducting material (YBCO), where the parameter  $\delta$  aptly signifies the presence of oxygen deficiency within the compound (Howe *et al.*, 2014).

Since its initial discovery, the Yttrium barium Copper Oxide (YBCO) compound has occupied a position of remarkable importance, driven by the overarching goal of realizing a superconductor capable of efficient operation at room temperature (Lilia *et al.*, 2022). This scientific pursuit culminated in the classification of ceramic superconductors, with YBCO standing as a prominent archetype, introduced to the world during the mid-20th century (Hilo *et al.*, 2022).

The structural architecture of YBCO unfolds through a meticulously arranged array of unit cells, characterized by dual Barium oxide planes flanking two  $\text{CuO}_2$  planes, with an intervening yttrium plane (Liang *et al.*, 2006). This precise arrangement forms the cornerstone of YBCO's intricate structural framework.

Amplifying the complexity of this structural foundation is the delicate interplay between the oxygen content nestled within the lattice and the temperature variations introduced during the heat treatment process. This dynamic interrelationship plays a pivotal role in sculpting the crystal structure and governing the dynamic conductivity of the YBCO system (Asikuzum *et al.*, 1987). Notably, the YBCO system exhibits an impressive sensitivity to varying oxygen levels, with even minor deviations leading to profound transformations in its electronic and superconducting properties.

The symbiotic interplay between oxygen concentration and heat treatment temperature elegantly choreographs the arrangement of atoms within the YBCO lattice. This intricate dance extends beyond mere atomic positioning, influencing vibrational energy states and electron mobility throughout the material. As a result, these interdependent factors wield significant influence over the symphony of superconducting behavior performed by YBCO, ultimately unveiling its extraordinarily high-temperature superconducting prowess.

In essence, the intricate interplay between structural and conductive properties within the YBCO system underscores the profound relationship linking atomic arrangement, oxygen levels, and superconducting performance. This deep understanding of the material's underlying dynamics plays a pivotal role in harnessing its potential across a wide spectrum of applications and advancing the boundaries of superconducting technology.

The term "super-conductor YBCO-123" serves as a distinctive emblem encapsulating the singular identity of  $\text{YBa}_2\text{Cu}_3\text{O}_{7-\delta}$ , with the symbol " $\delta$ " portraying the captivating presence of oxygen deficiency. This terminological insight underscores the intricate interplay of compositional elements and their profound influence on the material's exceptional superconducting properties.

Within the realm of scientific exploration, the panorama of metallic oxide nanostructures ignites an expansive confluence of curiosity, driven by the multifaceted promise they harbor across diverse domains. These domains encompass realms as varied as industrial purification processes, intricate biomedical applications (Akhavan *et al.*, 2014), and the horizons of nanoelectronics and optoelectronics (Meidanchi *et al.*, 2014). A defining attribute of these nano-scaled materials lies in their elevated surface-to-volume ratio, magnifying the significance of unsaturated and reactive surface atoms. This distinctive attribute imparts remarkable reactivity, forming the bedrock of their multifarious applications.

However, while the potential of nanostructures gleams, their journey towards realization within biological therapeutic applications is navigated with meticulous deliberation. Attributes spanning composition, size, crystal dimensions, morphology, stability, non-agglomeration, and biocompatibility converge as pillars of a meticulous evaluation. This comprehensive assessment emerges as an imperative endeavor, steering their harmonious integration within biological systems while safeguarding the sanctity of safety and efficacy.

Significantly, the realm of metallic and metal oxide nanoparticles has undergone a transformative renaissance, as they emerge as potent entities infused with intrinsic antibacterial properties. This inherent characteristic elevates their utility across a broad spectrum of applications, spanning realms from biomedicine to antibacterial coatings, pioneering water treatment solutions, and even unveiling innovative paradigms within the realm of food processing (Dastan *et al.*, 2017), (Hajipour *et al.*, 2012). This transformative potential illuminates a new era, wherein nanoparticles transcend their conventional roles to actively contribute to the advancement of human health, safety, and the ethos of environmental sustainability.

The conventional synthesis of oxide superconductor powder via solid-state reactions wrestles with a multitude of challenges, encompassing inhomogeneity, oversized particle dimensions, limited reproducibility, and extended heat-treatment protocols (Ramanligam *et al.*, 2016). To surmount these constraints and attain heightened uniformity, a diverse array of chemical methodologies has evolved (Rednorz *et al.*, 1986). In harmony with this evolution, the present study embarks on the chemical route to craft high-temperature superconductors (HTS), with a specific emphasis on the sol-gel approach. This method, initiated through alkoxides or acetates, offers a pragmatic and cost-effective avenue for producing superconducting  $\text{YBa}_2\text{Cu}_3\text{O}_{7-\delta}$  powder (Hasan *et al.*, 2021).

Within the scope of this paper, we meticulously detail the synthesis of YBCO nano powders, executed with precision using the sol-gel technique. This synthesis process is meticulously complemented by comprehensive structural and thermal characterizations that encompass techniques such as X-ray diffraction (XRD), scanning electron microscopy (SEM), and differential scanning calorimetry/thermogravimetric analysis (DSC/ATG). At the heart of this exploration lies the meticulous investigation of the antibacterial potential inherent in HTS YBCO nanoparticles. These nanoparticles are subjected to meticulous evaluation across a spectrum of concentrations, thoroughly tested against four distinct bacterial strains (0.01, 0.025, 0.05, and 0.1 mg/mL).

## 2. Materials and method

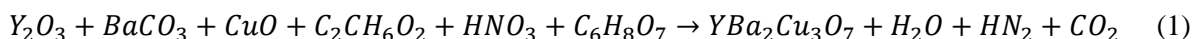
### 2.1 Synthesis of YBCO

The synthesis of YBCO nanoparticles was accomplished using a sol-gel process with the utilization of pure  $\text{Y}_2\text{O}_3$ ,  $\text{BaCO}_3$ , and  $\text{CuO}$ . The starting materials and their respective purities are listed in Table 1. Initial  $\text{CuO}$  powders with a composition of 78-79% copper was dissolved in nitric acid and then diluted using ionized water. To mitigate potential precipitation of  $\text{Ba}(\text{NO}_3)_2$ , the pH was adjusted to approximately 6 using ammonia (Tang *et al.*, 2013). The sol-gel process incorporated Citric Acid (CA) as a complexing agent and Ethylene Glycol (EG) as a polymerization agent.

**Table 1 – Departing precursors for YBCO synthesis**

| Element          | Chemical formula                 | Purity |
|------------------|----------------------------------|--------|
| Yttrium Oxide    | $\text{Y}_2\text{O}_3$           | 90%    |
| Citric acid      | $\text{C}_6\text{H}_8\text{O}_7$ | -      |
| Ethylene Glycol  | $\text{C}_2\text{H}_6\text{O}_2$ | -      |
| Nitric acid      | $\text{HNO}_3$                   | 69%    |
| Sodium hydroxide | $\text{NaOH}$                    | 90%    |
| Copper oxide     | $\text{CuO}$                     | 78-79% |
| Barium Carbonate | $\text{BaCO}_3$                  | 99.99% |

The weights of the starting precursors were calculated using the following equation:



The precursor weights used are presented in Table .2:

**Table .2 Precursor Weights and Volumes Used for YBCO Nanoparticle Synthesis.**

| Precursor   | Weight (g) | Volume (mL) |
|---|------------|-------------|
| Y(NO <sub>3</sub> )   | 8.24       | -           |
| Y <sub>2</sub> O <sub>3</sub>                               | 3.38       | -           |
| BaCO <sub>3</sub>   | 11.84      | -           |
| CuO   | 7.15       | -           |
| C <sub>2</sub> CH <sub>6</sub> O <sub>2</sub> (Citric Acid) | 5.18       | -           |
| HNO <sub>3</sub>  | -          | 27.6        |
| Ethylene Glycol   | -          | 15          |

For 1 hour and 30 minutes, the mixture was heated to 90 °C and stirred continuously with a magnetic agitator. Citric acid and metal cations then underwent a polymerization reaction to form the gel. This gel was thermoplastic, meaning it could be formed into a fiber like structure, similar to the previously reported Bi-base oxide. It was pulverized for 1.5 hours at 350°C in a muffle furnace to produce an ash like precursor. The powder was then calcined and milled twice at 850 °C and 920 °C.

## 2.2 Strains

The antibacterial activity of nanoparticles with a concentration of 10 mg/ml was evaluated against a set of bacteria including two Gram-negative strains (Escherichia coli ATCC 25922 and Pseudomonas aeruginosa ATCC 27853) as well as two Gram-positive strains (methicillin-resistant Staphylococcus aureus, MRSA ATCC 43300, and Staphylococcus epidermidis).

## 2.3 Well diffusion method

The well diffusion method was employed for antibacterial assessment. A Petri dish containing 20 mL of Muller-Hinton agar medium, previously inoculated with 0.1 mL of bacterial suspension, served as the substrate. A volume of 50 µL of the nanoparticle solution, with a concentration of 10 mg/mL, was carefully introduced into a 6-mm-diameter well made in the agar. The Petri dishes were then incubated at 37°C for a duration of 24 hours. The negative control utilized in the study was distilled water. To ensure the reliability of the results, all tests were conducted in triplicate, ensuring robustness and accuracy in the experimental setup (refer to Fig. 1 and Fig. 2).

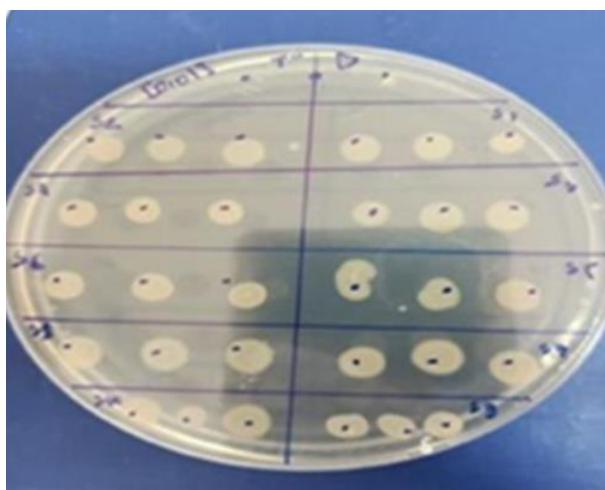


**Figure 1 - Results from spot assay**



Figure 2 – Result from well diffusion method

#### 2.4 Minimal concentration inhibition (MICs) on solid media

The agar dilution method was employed to determine the MICs for all nanoparticles on solid media. The MIC was defined as the lowest concentration of the agent that visibly inhibited bacterial growth after 24 hours of incubation at 37°C. To achieve high turbidity, isolates were cultured on Luria Bertani (LB) media and incubated at 37°C overnight. Colonies were resuspended in 0.9% saline solution to attain a concentration of 10<sup>8</sup> cells per milliliter or a turbidity equivalent to 0.5 McFarland standard. The Luria Bertani (LB) medium was supplemented with varying concentrations of nanoparticles, including 0.01, 0.025, 0.05, and 0.1 mg/mL. Subsequently, two microliters of each bacterial suspension were inoculated onto the plate. Distilled water served as the negative control, and all analyses were conducted in triplicate.

### 3. result and discussion

#### 3.1 SEM/EDAX Analysis

The microstructure of the samples was observed using a scanning electron microscope (SEM, QUANTA 250) equipped with a secondary electron detector. Figure 3 displays SEM micrographs of the YBCO powder, revealing grains that are distributed heterogeneously with irregular morphologies. In Figure 4, the SEM micrographs show well-diffused and relatively uniformly dispersed spherical nanoparticles. These nanoparticles tend to attach to one another, forming floral-like granules. This observation is consistent with findings reported in the literature (Slimani *et al.*, 2018).

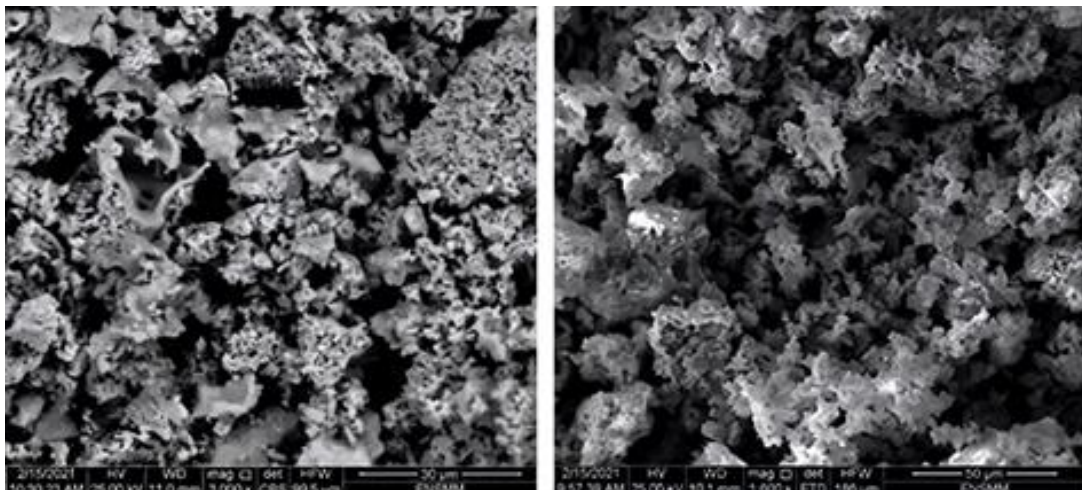


Figure 3 - SEM images of YBCO Powder.

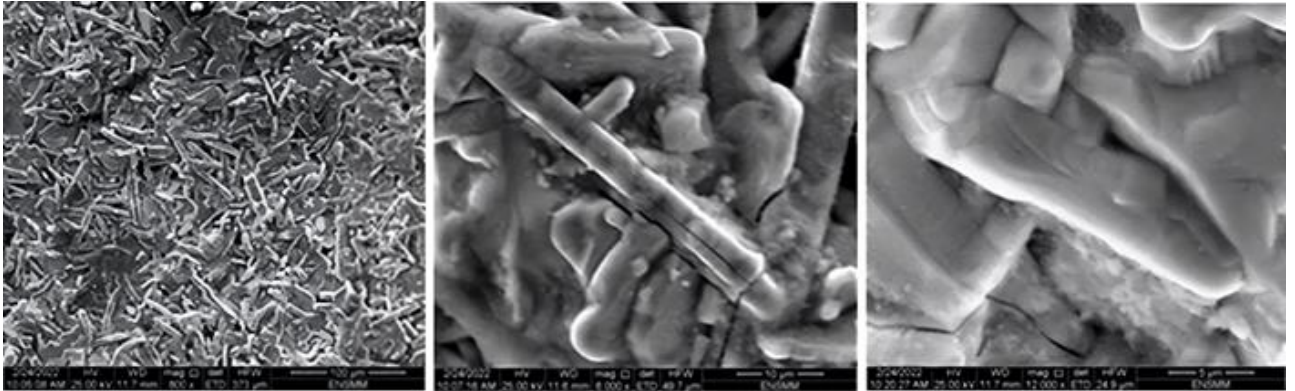


Figure 4 - SEM images of YBCO Pellet.

The elemental composition of YBCO-123 particles was determined by energy dispersive X-ray analysis to be 1:2:3 Yttrium: Barium: Copper (Fig. 5).

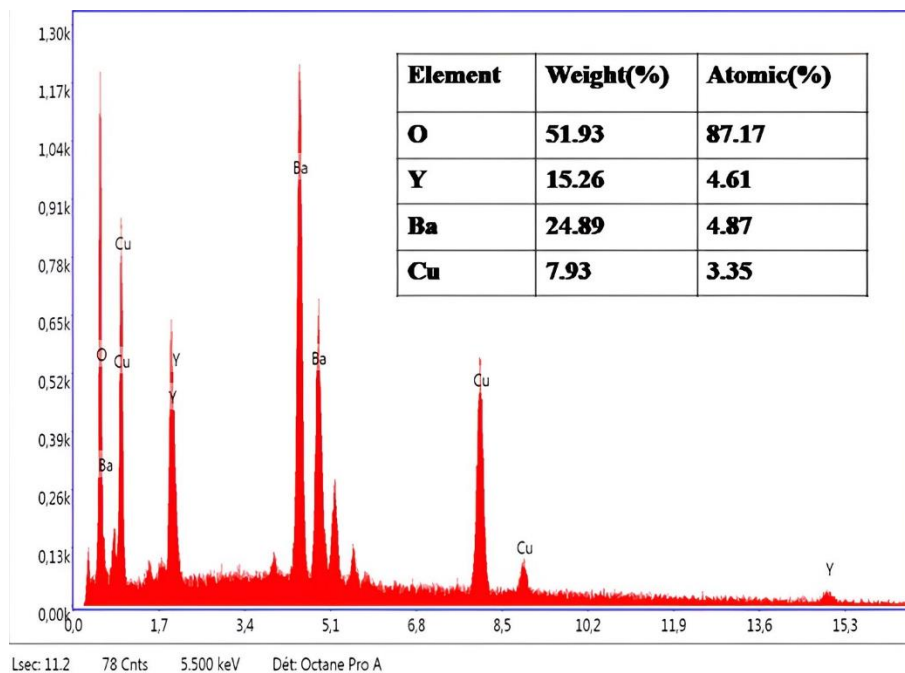


Figure 5 - The EDS pattern of YBCO.

### 3.2 X-Ray Diffraction

The X-ray diffraction (XRD) peaks of the HTS YBCO nanoparticles exhibited pronounced intensity and consistency in line with existing literature (Dadras *et al.*, 2018). In Figure 6, the optimized spectra for the YBCO nanoparticles are depicted following heat treatment of the nano powder sample. The XRD pattern of the YBCO-123 samples is presented in Figure 6 and has been analyzed with reference to card number JCPDS 40-0159 for  $\text{YBa}_2\text{Cu}_3\text{O}_7$ .

Upon indexing the YBCO diffraction pattern to the corresponding d-spacing values, all identified peaks were discernible. The sample's structure revealed a dominant phase exhibiting tetragonal symmetry, accompanied by a minor presence of the  $\text{Y}_2\text{BaCuO}_5$  phase. Notably, the primary peak of the Y-123 tetragonal phase at  $2\theta = 32.85$  corresponded to the (103) crystallographic planes. Furthermore, the Y-123 phase characterization encompassed peaks associated with the (100), (102), (004), (103), (005), (113), (200), (213), (220), and (303) planes.

In the orthorhombic phase of  $Y_2BaCuO_5$ , the lattice parameters were determined as  $a = 12.1760$ ,  $b = 5.6590$ , and  $c = 7.1340$ . Conversely, the hexagonal phase of Y-123 exhibited lattice parameters of  $a = 3.8630 = b$  and  $c = 11.6260$ . The orthorhombic phase of Y-211 was also identifiable through its associated peak at (311).

In the orthorhombic phase of  $Y_2BaCuO_5$ , the lattice parameters were  $a = 12.1760$ ,  $b = 5.6590$ , and  $c = 7.1340$ , whereas they were  $a = 3.8630 = b$  and  $c = 11.6260$  in the hexagonal phase of Y-123. The orthorhombic phase of Y-211 was also observed in peaks that were associated with it (311). The average Crystalline size of particles can be calculated from the (103) peak.

Calculations of the average crystalline size of particles were based on the (103) peak and utilized the Debye-Scherer equation:

$$D = \frac{k\lambda}{\beta \cdot \cos \theta} \quad (2)$$

Where:

- D represents the crystallite size.
- $K=0.9$  denotes Scherer's Constant
- $\lambda=0.15406 \text{ \AA}$  signifies the X-ray wavelength.
- $\beta$  stands for the full width at half-maximum (FWHM).

The calculated approximate crystallite size for the YBCO sample was found to be around 8.28 nm.

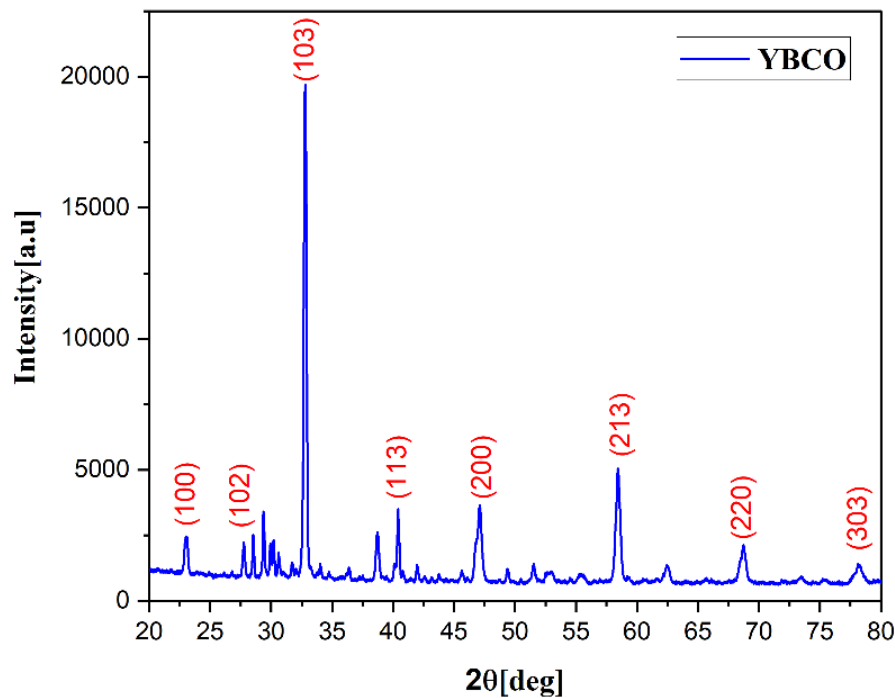


**Figure 6 - The X-ray diffraction patterns of YBCO by Sol-Gel Method.**

### 3.2 Thermal Analysis: DSC /TG

To refine the technical parameters and optimize the heat treatment process, the nanoparticles were subjected to differential scanning calorimetry (DSC) and thermogravimetric analysis (TG) (Fig. 7). These analyses were conducted to gather crucial information regarding temperature, heat-treatment duration, and sintering conditions (Jasim *et al.*, 2016). The heating rate employed for these analyses was set at  $10^\circ\text{C}/\text{min}$  to ensure consistent and controlled results.

The nanoparticle samples can be produced through two heat treatment processes. The exothermic peak indicates the occurrence of the first heat treatment at  $808^\circ\text{C}$ . The weight loss observed between  $800$  and  $900^\circ\text{C}$  signifies the crystallization of  $YBa_2Cu_3O_{7-\delta}$ . (Cui *et al.*, 2006). The second heat treatment at  $910^\circ\text{C}$  was required to phase crystallize YBCO and produce the final nanoparticles

sample of pure product. After 911 °C, endothermic peaks indicate when YBCO begins to melt and become unstable (Rasti *et al.*, 2020). Metal oxides undergo the conversion to the desired YBCO phase at sintering temperatures above 930 to 950°C in an air environment (Thuy *et al.*, 2012).

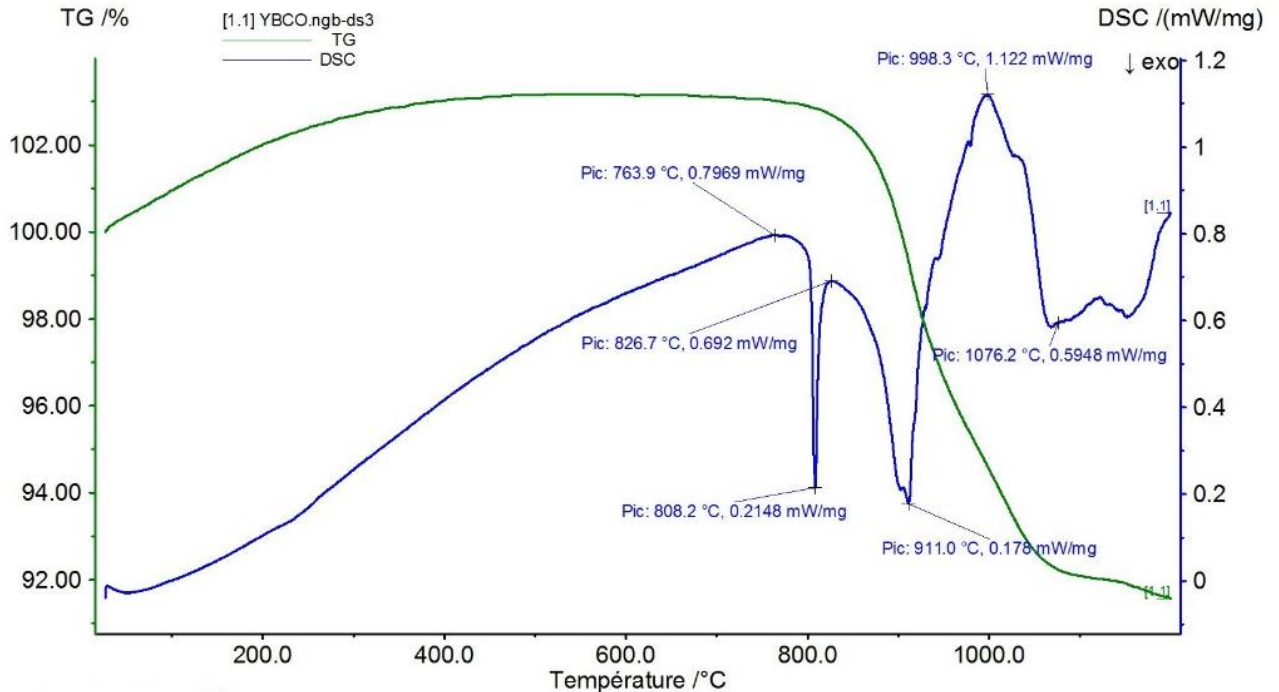


**Figure 7 - Thermo gravimetric analysis for YBCO sample.**

### 3.3 Antibacterial Activity

Nanoparticles with a concentration of 10 mg/mL were subjected to testing against two Gram-negative strains (*E. coli* ATCC 25922 and *Pseudomonas aeruginosa* ATCC 27853) and Gram-positive bacteria (methicillin-resistant *Staphylococcus aureus*, MRSA ATCC 43300, and *Staphylococcus epidermidis*). The impact of YBCO NPs was observed on *Staphylococcus epidermidis* and MRSA, which are Gram-positive strains. Conversely, the tested Gram-negative strains exhibited resistance to the effects of YBCO NPs. Notably, *Staphylococcus epidermidis* displayed greater sensitivity ( $12 \pm 0.2$  mm) to the action of YBCO NPs compared to MRSA ( $08 \pm 0.2$  mm) [Fig. 8].

This discrepancy might be attributed to the resistant nature of MRSA. Across concentrations of 0.01 mg/ml, 0.025 mg/ml, 0.05 mg/ml, and 0.1 mg/ml, YBCO NPs demonstrated negligible impact on the bacterial strains [Table 3 and Table 4]. The findings indicate that the tested strains exhibited resistance to high concentrations of 10, 0.01, 0.025, 0.05, and 0.1 mg/ml, which could potentially be linked to water permeability variations within Gram-positive bacteria. On the other hand, the resistance of Gram-negative bacteria could be attributed to their limited permeability to YBCO NPs.

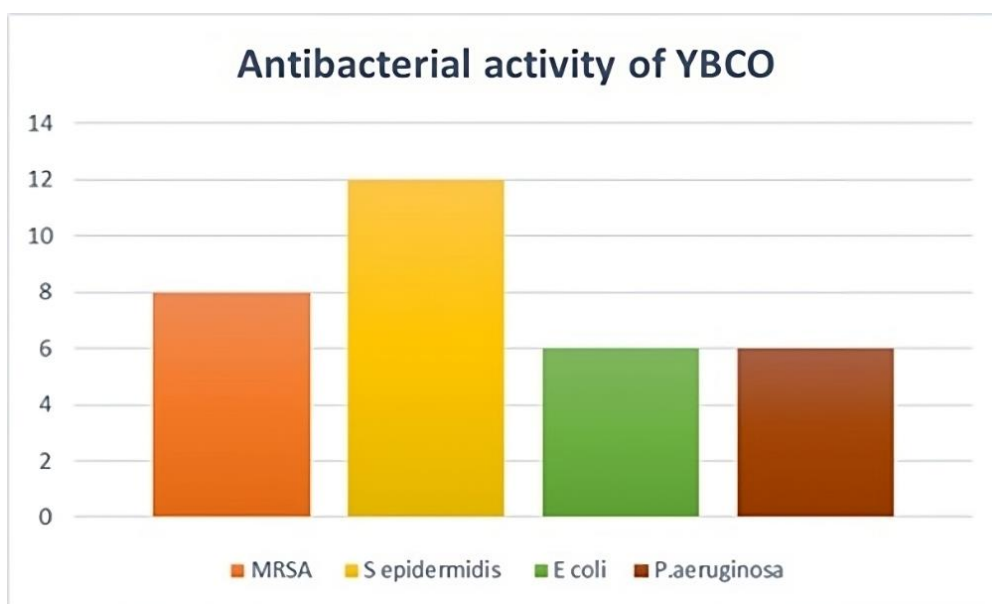


**Figure 8 - Antibacterial effect of YBCO NPs on Gram positive and Gram-negative strains.**

**Table 2: Obtained results from wells essays.**

| MRSA ATCC<br>43300 | <i>Staphylococcus</i><br><i>epidermidis</i> | <i>E. coli</i><br>ATCC 25922 | <i>Pseudomonas aeruginosa</i><br>ATCC 27853 |
|--------------------|---|------------------------------|---|
| 8±0.1mm            | 12±0.2mm                                    | 6mm±0.00mm                   | 6mm±0.00mm                                  |

**Table 3: obtained results from MIC essays**

| Concentrations<br>mg/mL | MRSA<br>ATCC 43300 | <i>Staphylococcus</i><br><i>epidermidis</i> | <i>E. coli</i><br>ATCC 25922 | <i>Pseudomonas aeruginosa</i><br>ATCC 27853 |
|-------------------------|--------------------|---|------------------------------|---|
| 0.01                    | +                  | +   | +                            | +   |
| 0.025                   | +                  | +   | +                            | +   |

#### 4. Conclusion

In this study, we address the critical need to discover novel antimicrobial agents from both natural and inorganic sources, a pivotal endeavor for advancing the development of sophisticated drugs and therapeutic solutions targeting microbial infections. This research focuses on harnessing the antimicrobial potential of YBCO NPs, marking an innovative frontier in the pursuit of effective treatments. The study underscores the urgency of exploring unconventional avenues to meet the challenges posed by microbial resistance. Employing the sol-gel method, renowned for its capacity to fabricate a diverse array of nanostructures characterized by exceptional attributes such as high porosity, controlled dimensions, and compact size, this investigation introduces an efficient strategy for synthesizing superconducting YBCO NPs. The success of the synthesis is evident through the generation of highly purified Y123 phase with minimal traces of Y-211, a confirmation supported by X-ray diffraction. Additionally, scanning electron microscopy unveils a distinct grain distribution, enriching our insight into the microstructure of the synthesized nanoparticles. The differential scanning calorimeter (DSC) and thermo gravimetric analysis (TG) contribute significantly to the comprehensive characterization of YBCO nano powder by revealing the optimal calcination and sintering temperatures. Intriguingly, the study unveils the antibacterial potency of

YBCO NPs, demonstrating susceptibility in Gram-positive strains, specifically *Staphylococcus epidermidis* and MRSA, while encountering resistance in a Gram-negative strain at higher concentrations. The upcoming study seeks to examine YBCO NPs under varying conditions, such as concentrations and temperatures. This ongoing investigation is vital to fully grasp their capabilities and potential applications in antimicrobial therapeutics, potentially leading to groundbreaking advancements in combatting microbial infections.

## References

- Akhavan, O., Meidanchi, A., Ghaderi, E., & Khoei, S. (2014). Zinc ferrite spinel-graphene in magneto-photothermal therapy of cancer. *Journal of Materials Chemistry B*, 2(21), 3306-3314. <https://doi.org/10.1039/c3tb21834a>.
- Asikuzun, E., Ozturk, O., Aydemir, G. A., & Tasci, A. T. (2019). The Effect of Zinc on the Structural, Electrical, and Mechanical Properties of YBCO-123 Superconducting Prepared by an Acetate-Based Sol-Gel Process. *Journal of Superconductivity Novel Magnetism*, 32, 3415-3423. <https://doi.org/10.1007/s10948-019-5127-z>.
- Bednorz, G. J. (1988). Miller, KA: *Z. Phys. B-Condensed Matter* 64, 189 (1986). *Rev. Mod. Phys.*, 60, 585. <https://doi.org/10.1103/RevModPhys.60.585>.
- Cui, X. M., Lyoo, W. S., Son, W. K., Park, D. H., Choy, J. H., Lee, T. S., & Park, W. H. (2006). Fabrication of YBa<sub>2</sub>Cu<sub>3</sub>O<sub>7-δ</sub> superconducting nanofibres by electrospinning. *Superconductor Science and Technology*, 19(12), 1264. <https://doi.org/10.1088/0953-2048/19/12/007>.
- Dadras, S., & Ghavamipour, M. (2018). Properties of YBCO high temperature superconductor synthesized by microwave oven. *Materials Research Express*, 5(1), 016001. <https://doi.org/10.1088/20531591/aaa5eb>
- Dastan, D., & Banpurkar, A. (2017). Solution processable sol-gel derived titania gate dielectric for organic field effect transistors. *Journal of Materials Science: Materials in Electronics*, 28, 3851-3859. <https://doi.org/10.1007/s10854-016-5997-9>.
- Gadzhimagomedov, S. K., Palchaev, D. K., Palchaev, N. A., Presnyakov, M. Y., & Rizahanov, R. N. (2019). Synthesis of YBCO nanopowders and properties of ceramics on their basis. *Crystallography Reports*, 64, 470-473. <https://doi.org/10.1134/S1063774519030052>.
- Hajipour, M. J., Fromm, K. M., Ashkarran, A. A., de Aberasturi, D. J., de Larramendi, I. R., Rojo, T., ... & Mahmoudi, M. (2012). Antibacterial properties of nanoparticles. *Trends in biotechnology*, 30(10), 499-511. <https://doi.org/10.1016/j.tibtech.2012.10.007>.
- Hasan, N., Hafeeth, H., & Ahmed, A. (2021). Synthesis and characterization of the bulk YBCO-target of superconducting material. *Materials Today: Proceedings*, 42, 2268-2272. <https://doi.org/10.1016/j.matpr.2020.12.314>.
- Hilo, M. H. M., & Shaheen, J. S. E. Synthesis and a Study the Optical Properties of Yttrium Barium Copper Oxide (YBCO) Using UV-Vis Techniques. <https://doi.org/10.11648/j.ijhep.20220901.14>.
- Howe, B. A., (2014). "Cornerstone: A Collection of Scholarly and Creative Works for Minnesota Crystal Structure and Superconductivity of YBa<sub>2</sub>Cu<sub>3</sub>O<sub>7-x</sub> Crystal Structure and Superconductivity," p. 69.
- Jasim, S. E., Jusoh, M. A., Hafiz, M., & Jose, R. (2016). Fabrication of superconducting YBCO nanoparticles by electrospinning. *Procedia engineering*, 148, 243-248. <https://doi.org/10.1016/j.proeng.2016.06.595>.
- Liang, D. A. (2006). Bonn, and WN Hardy. *Phys. Rev. B*, 73, 180505. <https://doi.org/10.1103/PhysRevB.73.180505>
- Lilia, B., Hennig, R., Hirschfeld, P., Profeta, G., Sanna, A., Zurek, E., ... & Valenti, R. (2022). The 2021 room-temperature superconductivity roadmap. *Journal of Physics: Condensed Matter*, 34(18), 183002. <https://doi.org/10.1088/1361-648X/ac2864>.

- Meidanchi, A., & Akhavan, O. (2014). Superparamagnetic zinc ferrite spinel–graphene nanostructures for fast wastewater purification. *Carbon*, 69, 230-238. <https://doi.org/10.1016/j.carbon.2013.12.019>.
- Ramalingam, B., Parandhaman, T., & Das, S. K. (2016). Antibacterial effects of biosynthesized silver nanoparticles on surface ultrastructure and nanomechanical properties of gram-negative bacteria viz. *Escherichia coli* and *Pseudomonas aeruginosa*. *ACS applied materials & interfaces*, 8(7), 4963-4976. <https://doi.org/10.1021/acsami.6b00161>.
- Rasti, M., & Mohammadzadeh, M. R. (2020). Fabrication of YBCO thin films by fluorine-free MOCSD method: influence of sintering near the melting point. *IEEE Transactions on Applied Superconductivity*, 30(6), 1-8. <https://doi.org/10.1109/TASC.2020.2982891>.
- Slimani, Y., Hannachi, E., Azzouz, F. B., & Salem, M. B. (2018). Impact of planetary ball milling parameters on the microstructure and pinning properties of polycrystalline superconductor Y3Ba5Cu8Oy. *Cryogenics*, 92, 5-12. <https://doi.org/10.1016/j.cryogenics.2018.03.010>.
- Sun, J. Z., Webb, D. J., Naito, M., Char, K., Hahn, M. R., Hsu, J. W. P., ... & Kapitulnik, A. (1987). Superconductivity and magnetism in the high- $T_c$  superconductor YBaCuO. *Physical review letters*, 58(15), 1574. <https://doi.org/10.1103/PhysRevLett.58.908>.
- Sunde, T. O. L., Grande, T., & Einarsrud, M. A. (2016). Modified Pechini synthesis of oxide powders and thin films. *Handbook of sol-gel science and technology*. <https://doi.org/10.1007/978-3-319-19454-7>.
- Tang, X., Zhao, Y., & Grivel, J. C. (2013). Influence of initial pH on the microstructure of YBa2Cu3O7-x superconducting thin films derived from DEA-aqueous sol-gel method. *Ceramics International*, 39(7), 7735-7741. <https://doi.org/10.1016/j.ceramint.2013.03.030>.
- Thuy, T. T., Herman, G., Lommens, P., & Driessche, I. V. (2012). Complexation behavior in aqueous edta sol-gel systems for the synthesis of YBa2Cu3O7-x high-temperature superconductors. *Journal of the Brazilian Chemical Society*, 23, 1289-1297. <https://doi.org/10.1590/S0103-50532012000700013>.